 FDMP, vol.1, no.4, pp.329-342, 2005

A High Resolution Pressure-Based Method for Compressible Fluid Flow

M.H. Djavareshkian[1]

Abstract: A pressure-based Euler scheme, based on a collocated grid arrangement is described. The newly developed algorithm has two new prominent features: (i) the use of normalized variables to bound the convective fluxes and (ii) the use of a high-resolution scheme in calculating interface density values to enhance the shock-capturing property of the algorithm. The algorithm is first tested for flows at different Mach numbers ranging from subsonic to supersonic on a bump in a channel geometry; then the results are compared with the corresponding ones obtained without the bounded scheme in the correction step. The output is also compared with data predicted by TVD schemes based on characteristic variables. These comparisons prove the boundedness in prediction and correction steps leads to sharp shocks and better resolution. The method is finally validated for external flow. The results of this scheme on C mesh are compared with another numerical solution and experiment data for the cases of incompressible, transonic and supersonic flows around airfoil NACA0012. According to the comparisons the resolution quality of present numerical model is considerable.

keyword: Normalized Variable Diagram, SBIC, Pressure-based, Aerodynamic Coefficients.

Nomenclature

A, D	= finite difference coefficients
$\tilde{a}$	= cell face area
a_η, a_ζ	= cell face area projection in the η and ζ directions respectively
e, w, n, s	= east, west, north and south cell faces
E, W, N, S	= East, West, North and South center cells
F	= mass flux
I	= flux
K	= a factor in SBIC scheme to determine a special scheme
M_∞	= free stream Mach number
q	= scalar flux vector
S_i^u, S^ϕ	= momentum and scalar source term respectively
T	= stress tensor
u, v	= velocity components in x and y directions, respectively
α	= angle of attack
Γ	= diffusivity coefficient
$\delta\upsilon$	= cell volume
μ	= dynamic viscosity
ρ	= density
$\tilde{\rho}$	= normalized density
ϕ	= scalar quantity
$\tilde{\phi}$	= normalized scalar quantity
η, ζ	= local coordinates
$\tilde{\eta}, \tilde{\zeta}$	= normalized local coordinates

1 Introduction

In many industrial applications (see, e.g., Deo, Starnes and Holzwarth (2001), Sujit (2004), Corol, Jerome and Katsuyoshi (2004) and Sean and Scott (2003)) the choice of the appropriate material for a given application requires "a priori" knowledge of the behavior and dynamics of fluids that are in contact with it. This is particularly true for aerospace applications where the optimization of the interplay between material strength and weight plays a role of crucial importance.

Computational fluid dynamic can be regarded as a feasible strategy for these purposes. Since both the transonic and supersonic regimes are very usual in aerospace application, there are many techniques for these regimes.

The numerical solution of the transonic and supersonic flows is usually carried out by time-marching methods that solve the set of the coupled system of equations governing the flux of mass, momentum and energy by means of accurate high-resolution schemes.

On the other hand, simulation of incompressible fluid flows with engineering interest is usually pursued with finite volume formulation, using primitive variables in conjunction with some variant of the semi-implicit pressure-correction method [Patankar and Spalding

[1] Tabriz University, Tabriz, Iran.

(1972)]. In this method the momentum equations are solved in a segregated fashion while an equation for a pressure-correction field is derived combining the discrete momentum and continuity equations [Patankar and Spalding (1972), Van Doormaal and Raithby (1984) and Issa (1985)].

Because this procedure in its standard form results in an elliptic equation for pressure (or pressure correction) it cannot "capture" the hyperbolic nature of the signal propagation in compressible transonic or supersonic flows.

Several attempts have been made by incompressible fluid flow numerical researchers, towards the unification of numerical methods developed for incompressible and compressible flows [Issa and Lockwood (1977), Van Doormaal, Raithby and McDonald (1987), Shyy (1988), Karki and Patankar (1989), McGuirk (1990) and Lien and leschziner (1993)]. In particular, great research efforts have been devoted to the development of the high-resolution schemes in pressure-based methods [Lien and leschziner (1993), Shyy and Thakur (1994), Thukur, Wright, Shyy, Liu, Ouyang and Vu (1996), Issa and Javareshkian (1998), Kobyashi and Pereira (1996) and Batten, Lien and Leschziner (1996)].

Leonard (1988) has generalized the formulation of the high-resolution flux limiter schemes using what is called the NVF (Normalized Variable Formulation). The NVF methodology has provided a good framework for development of high-resolution schemes that combine simplicity of implementation with high accuracy and boundedness. Gaskell and Lau (1988) introduced SMART (Sharp and Monotonic Algorithm for Realistic Transport) scheme that is combined with first and high order interpolation procedures based on NVD (Normalized Variable Diagram). The SFCD (Self Filtered Central Differencing) scheme was presented by Ziman (1991). Zhu and Rodi (1991) introduced the SOUCUP (Second-Order Upwind-Central differencing first-order Upwind) scheme. Darwish (1993) developed STOIC (Second and Third-Order Interpolation for Convection) scheme that is integrated from high order interpolation procedures to control convective terms. Van Leer's MUSCL (Monotone Upstream Scheme of Conservation Laws)(1974), Chakravarthy and Osher's OSHER (1983) and the MINMOD (minimum modulus) of Roe (1985) are other NVD schemes. A functional relationship based on normalized variable is given for all second and third order schemes with nonuniform grid in Darwish & Moukalled (1994).

The above NVD methods use different differencing schemes through the solution domain. The related procedure includes some kind of switching between the differencing schemes; switching introduces additional nonlinearity and instability in to the computation.

The worst case is that instead of a single solution for a steady state problem; the differencing scheme creates two or more unconverged solutions with a cyclic alternance between them. In such a case it is impossible to obtain a converged solution and convergence stalls at some level.

Non-discrete functions are used in the Van Leer's CLAM (Curved Line Advection Method) [Van Leer (1974)], Leonard's EULER [Leonard (1983)] and the SBIC (Second and Blending Interpolation Combine) scheme [Djavareshkian (2001)] and schemes based on the convection boundedness criteria (CBC). The later scheme is simply and extension to non-uniform meshes by Jasak, Weller and Gosman (1999). In all of these methods, the NVD scheme is applied in the prediction step.

The newly developed algorithm discussed in the present article has two new features: (i) the use of normalized variables to bound the convective fluxes in prediction step and (ii) the use of a high-resolution scheme in calculating interface density values to enhance the shock-capturing property of the algorithm in the correction stage. The algorithm is tested for incompressible and compressible as well as internal and external flows. The results have been compared with the corresponding algorithm without bounded scheme. The results have also been compared with predicted data by TVD schemes based on characteristic variables.

2 Governing Equations

The basic equations, which describe conservation of mass, momentum and scalar quantities, can be expressed in Cartesian tensor form as

$$\frac{\partial \rho}{\partial t} + \frac{\partial (\rho u_j)}{\partial x_j} = 0 \tag{1}$$

$$\frac{\partial (\rho u_i)}{\partial t} + \frac{\partial (\rho u_i u_j - T_{ij})}{\partial x_j} = S_i^u \tag{2}$$

$$\frac{\partial (\rho \phi)}{\partial t} + \frac{\partial (\rho u_j \phi - q_j)}{\partial x_j} = S^\phi \tag{3}$$

The stress tensor and scalar flux vector are usually expressed in terms of basic dependent variable. The stress

tensor for a Newtonian fluid is

$$T_{ij} = -p\delta_{ij} - \frac{2}{3}\mu \frac{\partial u_k}{\partial x_k}\delta_{ij} + \mu\left(\frac{\partial u_i}{\partial x_j} + \frac{\partial u_j}{\partial x_i}\right) \tag{4}$$

The scalar flux vector usually given by the Fourier-type law:

$$q_j = \Gamma_\phi\left(\frac{\partial \phi}{\partial x_j}\right) \tag{5}$$

3 Discretization

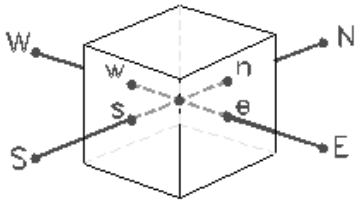

Figure 1 : Typical grid – point cluster and control volume

The discretization of the above differential equations is carried out using a finite-volume approach. First, the solution domain is divided into a finite number of discrete volumes or cells, where all variables are stored (at their geometric centers, see e.g. Fig. 1). The equations are then integrated over all the control volumes by using the Gaussian theorem. The discrete expressions are presented with reference to only one face of the control volume, namely,*e* for the sake of brevity.

For any variable ϕ (which may also stand for the velocity components), the result of the integration yields

$$\frac{\delta \upsilon}{\delta t}\left[(\rho\phi)_p^{n+1} - (\rho\phi)_p^n\right] + I_e - I_w + I_n - I_s = S_\phi \delta\upsilon \tag{6}$$

Where$I$'s are the combined cell-face convection,I^c and diffusion,I^D fluxes. The diffusion flux is approximated by central differences and can be written for cell-face e of the control volume in Fig. 1 as:

$$I_e^D = D_e(\phi_p - \phi_E) - S_e^\phi \tag{7}$$

WhereS_e^ϕstands for cross derivative arising from mesh nonorthogonality. The discretization of the convective flux, however, requires special attention and is the core of the various schemes developed in the literature. A representation of the convective flux for cell-face e is:

$$I_e^c = (\rho.V.\mathrm{A})_e\phi_e = F_e\phi_e \tag{8}$$

The value of ϕ_e is not known and should be estimated by interpolation, from the values at neighboring grid points. The expression for ϕ_e is determined by the SBIC scheme, that is based on the NVD technique, used for interpolation from the nodes E, P and W. The expression ϕ_e for positive direction of the velocity can be written as

$$\phi_e = \phi_W + (\phi_E - \phi_W)\cdot\phi_e \tag{9}$$

The functional relationship used in the SBIC scheme for $\tilde{\phi}_e$ is given by:

$$\begin{aligned}
&\tilde{\phi}_e = \tilde{\phi}_P \quad \text{if } \tilde{\phi}_C \notin [0,1]\\
&\tilde{\phi}_e = -\frac{\tilde{\eta}_P - \tilde{\eta}_e}{K(\tilde{\eta}_P - 1)}\tilde{\phi}_P^2 + \left(1 + \frac{\tilde{\eta}_P - \tilde{\eta}_e}{K(\tilde{\eta}_P - 1)}\right)\tilde{\phi}_P\\
&\qquad\qquad \text{if } 0 \le \tilde{\phi}_P \le K\\
&\tilde{\phi}_e = \frac{\tilde{\eta}_P - \tilde{\eta}_e}{\tilde{\eta}_P - 1} + \frac{\tilde{\eta}_e - 1}{\tilde{\eta}_P - 1}\tilde{\phi}_P \quad \text{if } K < \tilde{\phi}_P \le 1
\end{aligned} \tag{10}$$

where

$$\tilde{\phi}_P = \frac{\phi_P - \phi_W}{\phi_E - \phi_W}, \quad \tilde{\phi}_e = \frac{\phi_e - \phi_W}{\phi_E - \phi_W}$$
$$\tilde{\eta}_e = \frac{\eta_e - \eta_W}{\eta_E - \eta_W}, \quad \tilde{\eta}_P = \frac{\eta_P - \eta_W}{\eta_E - \eta_W}$$

The limits on the selection of K can be determined in the following way. Obviously the lower limit is$K = 0$ which would represent switching between upwind and central differencing. This is not favorable because it is essential to avoid abrupt switching between the schemes in order to achieve the converged solution. The value of K should be kept as low as possible in order to achieve maximum resolution.

When all other fluxes at the various cell faces are calculated according to the equations (7), (8), (9), (10) and introduced into the equation (6), the discretized equations resulting from each approximation take the form:

$$A_P.\phi_P = \sum_{m=E,W,N,S} A_m.\phi_m + S'_\phi + S_{dc} \tag{11}$$

WhereA's are the convection-diffusion coefficients. The term S'_ϕ in Eq. (11) contains quantities arising from nonorthogonality, numerical dissipation terms and external

sources, and $(\rho\delta\upsilon/\delta t)\phi_P$ of the old time-step/iteration level (for time dependent equation). For the momentum equations it is easy to separate the pressure-gradient source from the convected momentum fluxes. S_{dc} is the contribution due to the correction procedure. The convection-diffusion coefficients for positive direction of the velocity are:

$$\begin{cases} A_E = D_e \\ A_W = D_w + F_w \\ A_N = D_n \qquad\qquad \tilde{\phi}_P \notin [0,1] \\ A_S = D_s + F_s \\ A_P = A_E + A_W + A_N + A_S \end{cases}$$

$$\begin{cases} A_E = D_e - (\tilde{\eta}_P - \tilde{\eta}_e)/(\tilde{\eta}_P - 1) \times F_e \\ A_W = D_w + (1 - (\tilde{\eta}_W - \tilde{\eta}_w)/(\tilde{\eta}_W - 1)) \times F_w \\ A_N = D_n - (\tilde{\zeta}_P - \tilde{\zeta}_n)/(\tilde{\zeta}_P - 1) \times F_n \\ A_S = D_s + (1 - (\tilde{\zeta}_S - \tilde{\zeta}_s)/(\tilde{\zeta}_S - 1)) \times F_s \\ A_P = A_E + A_W + A_N + A_S \qquad K < \tilde{\phi}_P \le 1 \end{cases}$$

$$\begin{cases} A_E = D_e - \frac{\tilde{\phi}_{P\eta}}{K}(\frac{\tilde{\eta}_P - \tilde{\eta}_e}{\tilde{\eta}_P - 1}) \times F_e \\ A_W = D_w + (1 - \frac{\tilde{\phi}_{W\eta}}{K}(\frac{\tilde{\eta}_W - \tilde{\eta}_w}{\tilde{\eta}_W - 1})) \times F_w \\ A_N = D_n - \frac{\tilde{\phi}_{P\zeta}}{K}(\frac{\tilde{\zeta}_P - \tilde{\zeta}_n}{\tilde{\zeta}_P - 1}) \times F_n \\ A_S = D_s + (1 - \frac{\tilde{\phi}_{S\zeta}}{K}(\frac{\tilde{\zeta}_S - \tilde{\zeta}_s}{\tilde{\zeta}_S - 1})) \times F_s \\ A_P = A_E + A_W + A_N + A_S \qquad 0 \le \tilde{\phi}_P \le K \end{cases} \tag{12}$$

With higher-order schemes, the evaluation of ϕ_e may involve a large number of neighboring grid points. Therefore, in order to simplify the solution of the resulting system of algebraic equations, a compacting procedure is usually used. The correction procedure of Rubin and Khosla (1982) adopted in this work, is based on replacing the convective flux at control volume face by an equivalent flux given by

$$I_e^c = F_e\phi_e = F_e\phi_e^U - F_e(\phi_e^U - \phi_e) \tag{13}$$

Where the superscript U denotes values obtained by the first-order upwind scheme and ϕ_e represents the cell face value computed by the SBIC scheme. For the positive direction of the velocity, ϕ_e^U on the cell face e will be equal to ϕ_P. With the preceding assumption, each discretized equation contains five unknowns (in two dimensions), and the matrix of coefficients of the resulting system of equations is pentadiagonal and always diagonally-dominated since it come from the first order upwind scheme.

4 Solution algorithm

The set of (11) is solved for the primitive variables (velocity components and energy) together with the continuity equation by means of pressure-based implicit sequential solution methods. The technique used is the SIMPLE scheme presented below. In this technique, however, the methodology has to be adapted in order to handle the way in which the fluxes are computed in Eq. (8).

The adapted SIMPLE scheme consists of a predictor and corrector sequence of steps at each iteration. The predictor step solves the implicit momentum equation using the old pressure field. Thus, for example, for the u component of velocity, the momentum predictor stage can be written as

$$u^* = H(u^*) - D\nabla p^o + S'_u \tag{14}$$

where

$$H(u^*) = (A_E u_E^* + A_W u_W^* + A_N u_N^* + A_S u_S^*)/A_P \tag{15}$$

and

$$\begin{aligned} -D\nabla p^o &= -(\frac{\partial p^o}{\partial x})_P.\delta v/A_P \\ &\equiv (-a_\eta.(p_e^o - p_w^o) + a_\zeta.(p_n^o - p_s^o))/A_P \end{aligned} \tag{16}$$

Superscripts * and o denote intermediate and previous iteration values, respectively. Note that the pressure-gradient term is now written explicitly; it is extruded from the total momentum flux by simple subtraction and addition. The corrector-step equation can be written as

$$u^{**} = H(u^*) - D\nabla p^* + S'_u \tag{17}$$

Equations (14) and (17) can be written for the $e$cell-face velocities as:

$$u_e^* = \tilde{H}(u^*) - \tilde{D}\tilde{\nabla}p^o + \tilde{S}'_u \tag{18}$$

$$u_e^{**} = \tilde{H}(u^*) - \tilde{D}\tilde{\nabla}p^* + \tilde{S}'_u \tag{19}$$

Hence, from (18) and (19)

$$u_e^{**} - u_e^* = -\tilde{D}\tilde{\nabla}(p^* - p^o) \;\; or \;\; \delta u = -\tilde{D}\tilde{\nabla}\,\delta p \tag{20}$$

Now the continuity equation demands that

$$\nabla(\rho^* u^{**}) = 0 \tag{21}$$

For compressible flows it is essential to account for the effect of change of density on the mass flux as the pressure changes. This is accounted for by linearizing the mass fluxes [Karki and Patankar (1989)]

$$\rho^* u^{**} \approx \rho^o u^* + (\rho^o)^{HR}\,\delta u + u^*\delta\rho \tag{22}$$

or

$$\rho^* u^{**} \approx \rho^o u^* - (\rho^o)^{HR} D\nabla\delta p + u^*(\frac{d\rho}{dp})\,\delta p \tag{23}$$

where equation (20), invoked to eliminate δu and $\delta\rho$, is related to δp by the appropriate equation of state. Substitution of (23) into (21) yields a pressure-correction equation in the form

$$\begin{aligned} A_P.\delta p_P^* = A_E.\delta p_E^* + A_W.\delta p_W^* + A_N.\delta p_N^* \\ + A_S.\delta p_S^* + S_P \end{aligned} \tag{24}$$

Where S_P is the finite difference expression of$\nabla(\rho^o u^*)$, that vanishes when the solution is converged. The A coefficients in (24) take the form (the expression for A_E is given as an example)

$$A_E = (\rho_e^o)^{HR}\,(\tilde{a}\tilde{D})_e - \lambda_e(\tilde{a}u^*)_e.(\frac{d\rho}{dp})_e \tag{25}$$

where

$$(\rho_e^o)^{HR} = \rho_W^o + \tilde{\rho}_e^o(\rho_E^o - \rho_W^o) \tag{26}$$

and

$$\tilde{\rho}_e^o = \begin{cases} \tilde{\rho}_P^o & \tilde{\rho}_P^o \notin [0,1] \\ -\frac{\tilde{\eta}_P-\tilde{\eta}_e}{K(\tilde{\eta}_P-1)}\tilde{\rho}_P^{o\,2} + (1+\frac{\tilde{\eta}_P-\tilde{\eta}_e}{K(\tilde{\eta}_P-1)})\tilde{\rho}_P^o & 0 \le \tilde{\rho}_P^o \le K \\ \frac{\tilde{\eta}_P-\tilde{\eta}_e}{\tilde{\eta}_P-1} + \frac{\tilde{\eta}_e-1}{\tilde{\eta}_P-1}\tilde{\rho}_P^o & K < \tilde{\rho}_P^o \le 1 \end{cases} \tag{27}$$

Where λ is a factor whose role is explained subsequently. Because the mass flux at a cell face is computed directly from nodal values of density and velocity, the cell-face values of $(\rho_e^o)^{HR}$and u_e^* in (25) are not readily available. To compute those values, assumptions concerning the variations of ρneed to be made. For example, $\lambda_e$is calculated according to Eq. (28); it depends on the flux direction and the normalized density at nodal value as:

$$\lambda_e = \begin{cases} 1 & if\ F_e > 0\ \ and\ \ \tilde{\rho}_P \notin [0,1] \\ 0 & if\ F_e < 0\ \ and\ \ \tilde{\rho}_P^o \notin [0,1] \\ 1-(1-\frac{\tilde{\eta}_P-\tilde{\eta}_e}{\tilde{\eta}_P-1})\frac{\tilde{\rho}_P}{K} & if\ F_e < 0\ \ and\ \ 0 \le \tilde{\rho}_P^o \le K \\ \frac{\tilde{\eta}_P-\tilde{\eta}_e}{\tilde{\eta}_P-1}\frac{\tilde{\rho}_{\eta P}}{K} & if\ F_e > 0\ \ and\ \ 0 \le \tilde{\rho}_P^o \le K \\ \frac{\tilde{\eta}_P-\tilde{\eta}_e}{\tilde{\eta}_P-1} & if\ K < \tilde{\rho}_P^o \le 1 \end{cases} \tag{28}$$

On the other hand, when $\tilde{\rho}_P^o \notin [0,1]$, then $\lambda_e$would take the value of 1 when u is positive; otherwise it would be zero. Alternatively, if$K < \tilde{\rho}_P^o \le 1$, a central difference formula is used. For $0 \le \tilde{\rho}_P^o \le K$ and according to the flow direction, it is calculated by SBIC scheme, first and second order interpolation procedures.

The structure of the coefficients in eq. (24) simulates the hyperbolic nature of the equation system. Indeed, a closer inspection of expression (25) reveals an "upstream bias" of the coefficients (A decreases as u increases), and this bias is proportional to the square of the Mach number. It should be also noted that the coefficients tend to their incompressible form in the limit of zero Mach number.

The overall solution procedure follows the same steps as in the standard SIMPLE algorithm, with the exception of the solution of the hyperbolic-like pressure-correction (24). To ensure convergence of the iteration process, under-relaxation factors between 0.1 and 0.2 for pressure correction and between 0.2 and 0.5 for the other variables are employed.

5 Results

Computational results are shown in subsequent figures for a series of test cases. The results of internal subsonic, transonic and supersonic flow calculations over a bump in a channel as well as external incompressible, transonic and supersonic compressible flow calculations are presented.

For these tests, at the inlet of the domain all flow vari-

ables are specified if supersonic flow is considered. For subsonic inlet flow, stagnation pressureP_o, stagnation temperature T_o and the inlet angle are specified. At the outlet, all the flow variables are given by extrapolation for supersonic velocity, whereas the static pressure is fixed in the case of a subsonic outlet.

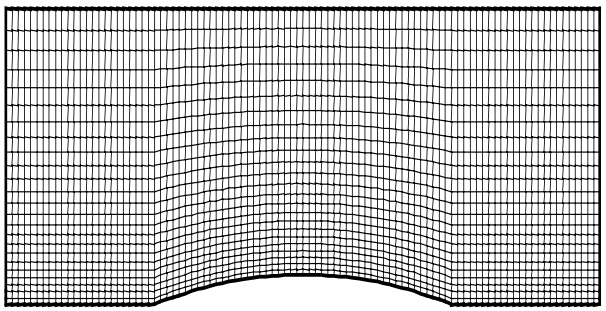

Figure 2 : Bump Geometry

For internal flows, a non-uniform grid of 98×25 in which the grid lines are closely packed in and near the bump region is chosen (Fig. 2) and slip boundary conditions are used on the upper and lower walls.

In order to assess the boundedness properties in the prediction and correction steps of the algorithm, three schemes are chosen. 1- the first order upwind scheme is used to calculated velocity components, energy and density ($D-Upwind$ and $M-Upwind$) 2- the SBIC scheme is used to evaluate velocity components and energy, and the density is calculated by first order upwind schemes ($M-SBIC$and $D-Upwind$) 3- the SBIC scheme is applied to calculate the above-mentioned parameters ($M-SBIC$and $D-SBIC$).

In the first test, static to stagnation pressure ratio was selected in order to give a Mach number of 0.5 at inlet. The value of the K in SBIC scheme for this case is 0.1. The Mach number distribution on the lower and upper walls for the three present schemes are compared with TVD scheme [Issa and Javareshkian (1998)] in Figs. 3(a-c). As it is seen, when the SBIC scheme is used to calculate the density on the cell face for subsonic flows, the results do not change.

The results of transonic flow with inlet Mach number equal to 0.675 for the same test case and schemes are shown in Figs. 4(a-h). The Mach number and pressure ratio distributions on the lower and upper walls for three

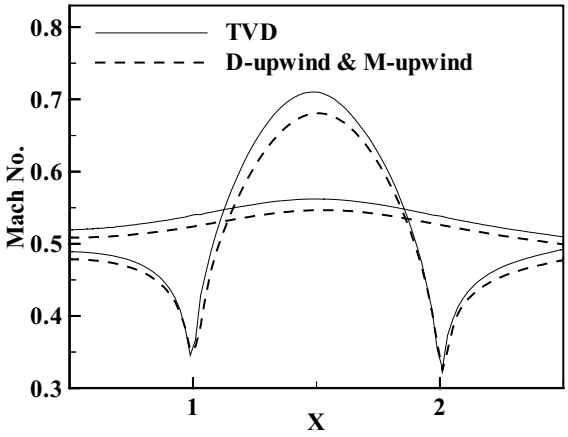

(a) Mach number along the walls

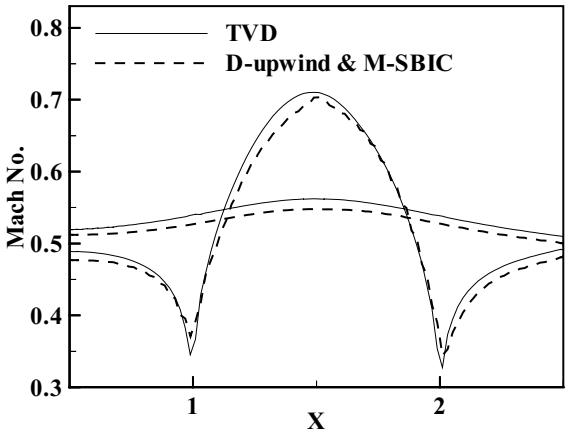

(b) Mach number along the walls

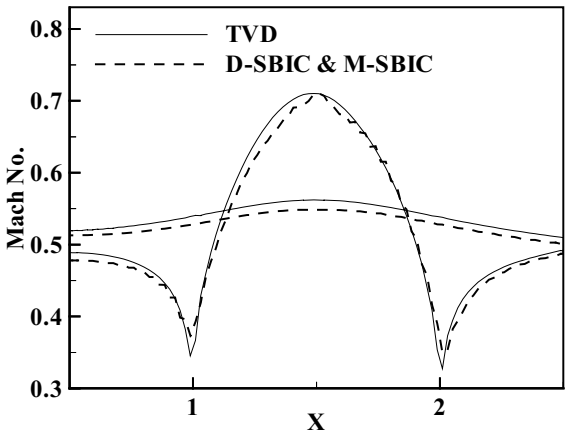

(c) Mach number along the walls

Figure 3 : Subsonic flow over 10% thick bump, inlet M_∞ =0.5

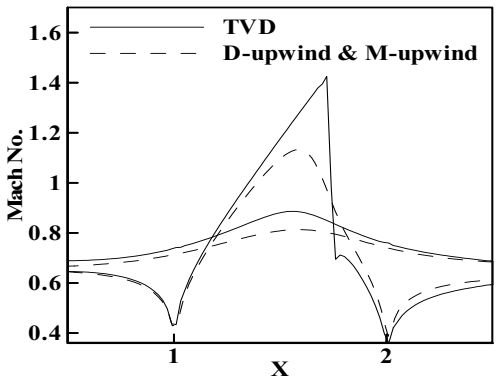

(a) Mach number along the walls

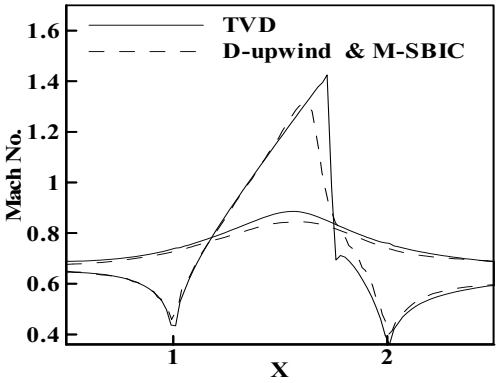

(b) Mach number along the walls

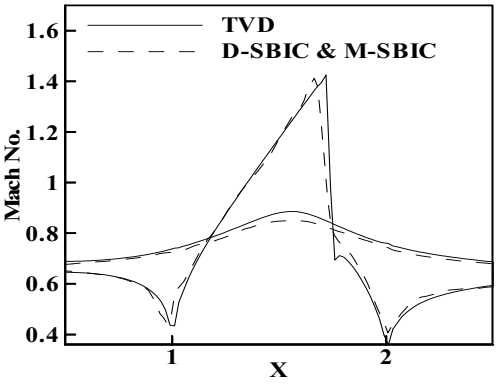

(c) Mach number along the walls

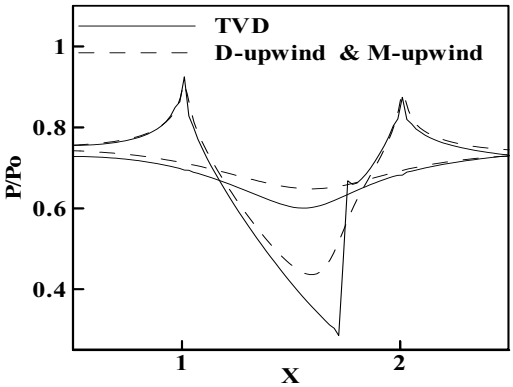

(d) Pressure ratio along the walls

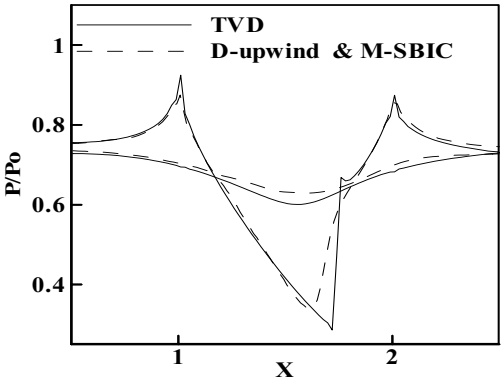

(e) Pressure ratio along the walls

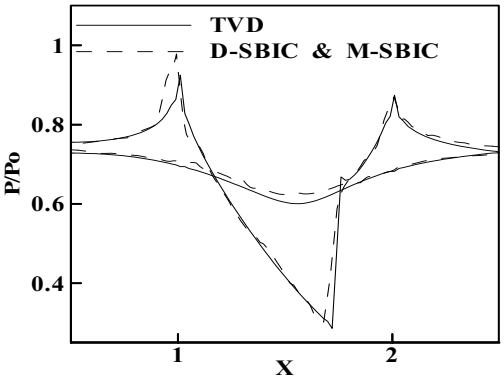

(f) Pressure ratio along the walls

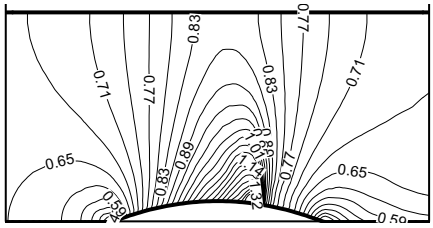

(g) Mach contours (D-SBIC & M-SBIC)

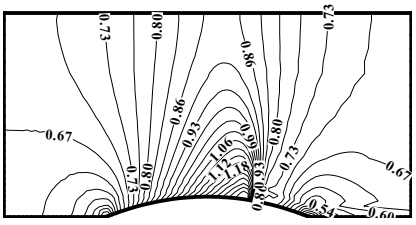

(h) Mach contours (TVD scheme)

Figure 4 : Transonic flow over 10% thick bump, inlet M_∞=0.675

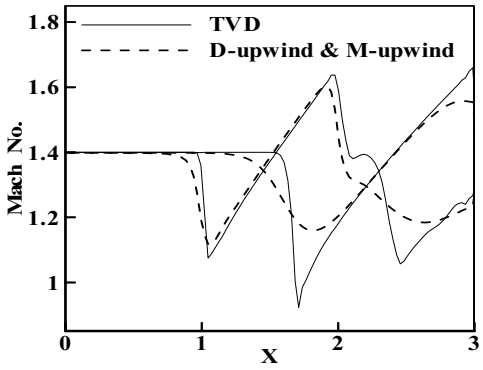

(a) Mach number along the walls

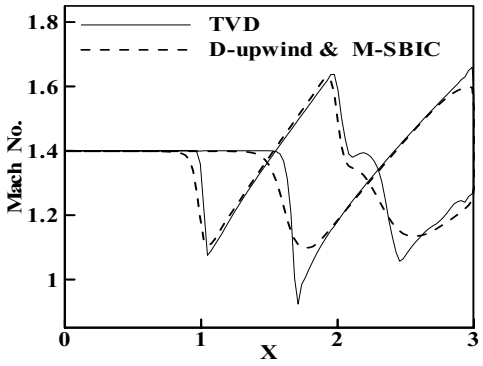

(b) Mach number along the walls

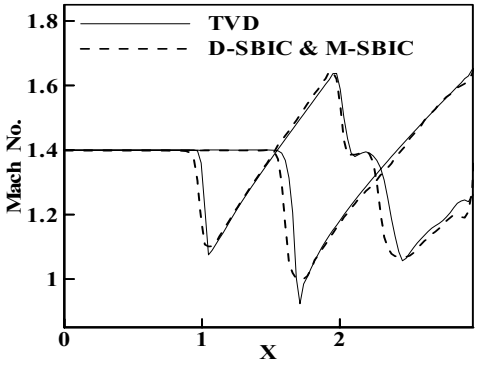

(c) Mach number along the walls

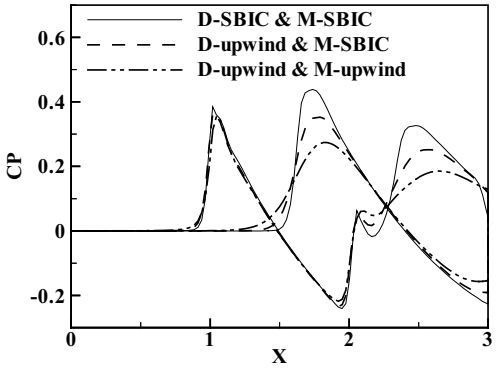

(d) Pressure ratio along the walls

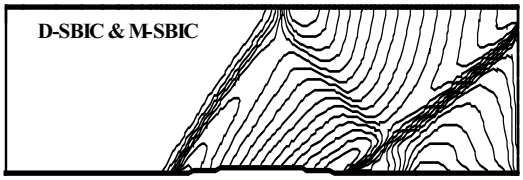

(e) Mach contours

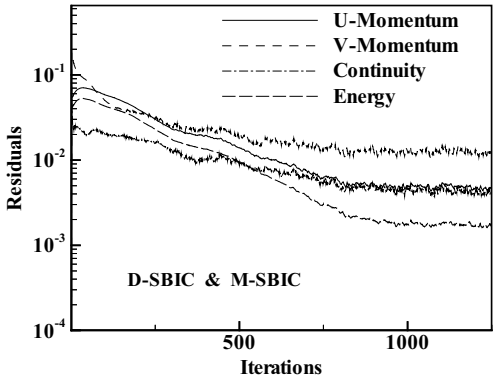

(f) Convergence histories

Figure 5 : Supersonic flow over 4% thick bump, inlet M_∞=1.4

present schemes are compared with TVD schemes [Issa and Javareshkian (1998)] in Figs. 4(a-c) and 4(d-f), respectively. Figs 4(g,h) show the Mach contours for the present and the TVD schemes. It can be observed that when the SBIC scheme is applied to calculate velocity components, energy and density, in prediction and correction steps, the transonic shock is sharper.

The third case is supersonic flow over 4% thick bumps on a channel wall. The computations were performed on a grid90×30. Figs 5(a,b,c) and 5(d) show the Mach number and pressure ratio distribution on the upper and lower surfaces for the three present schemes. These results are also compared with the TVD [Issa and Javareshkian (1998)] prediction. Such a comparison shows the development of present scheme in prediction and correction steps leads to better resolution for supersonic shock

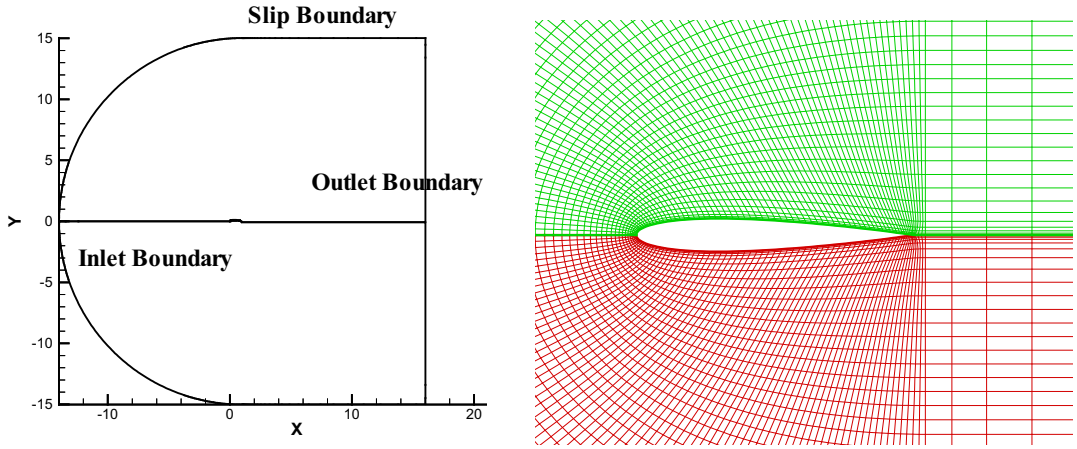

(a) (b)

Figure 6 : a) Domain b) Part of the C grids used for the NACA 0012 airfoil

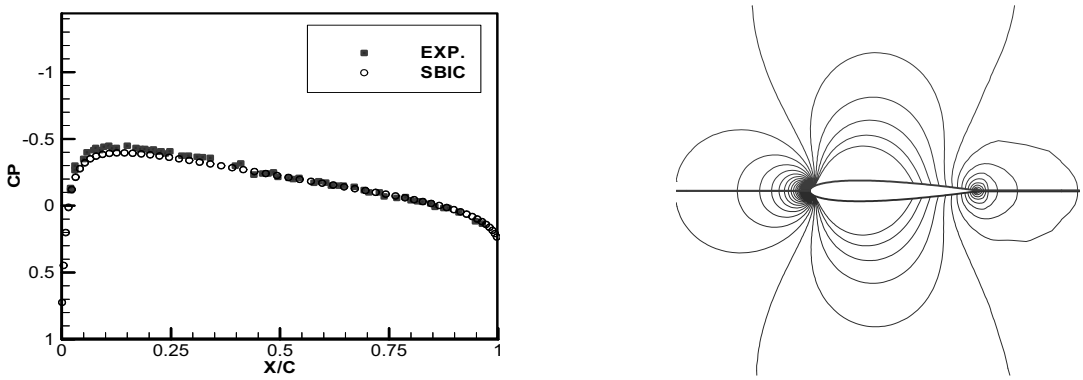

(a) (b)

Figure 7 : a) Surface pressure ratio b) Mach contour for $\alpha = 0$ and $M_\infty = 0.281$

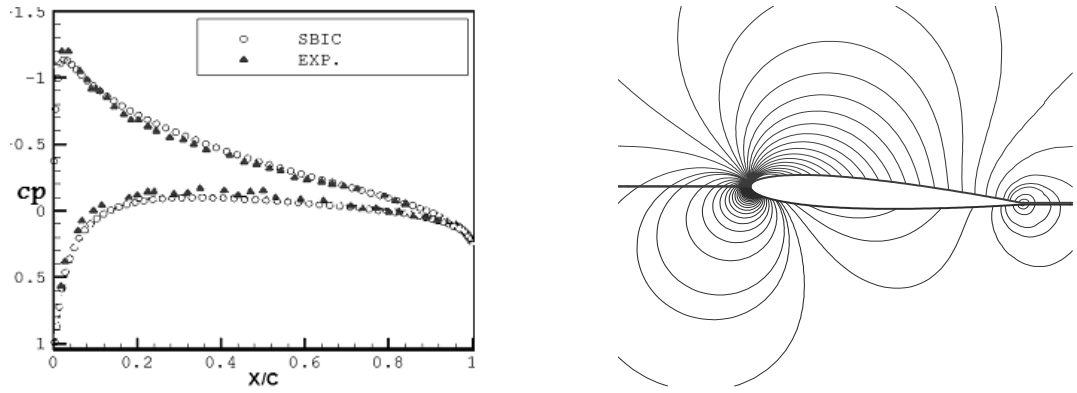

(a) (b)

Figure 8 : a) Surface pressure ratio b) Mach contour for $\alpha = 4$ and $M_\infty = 0.281$

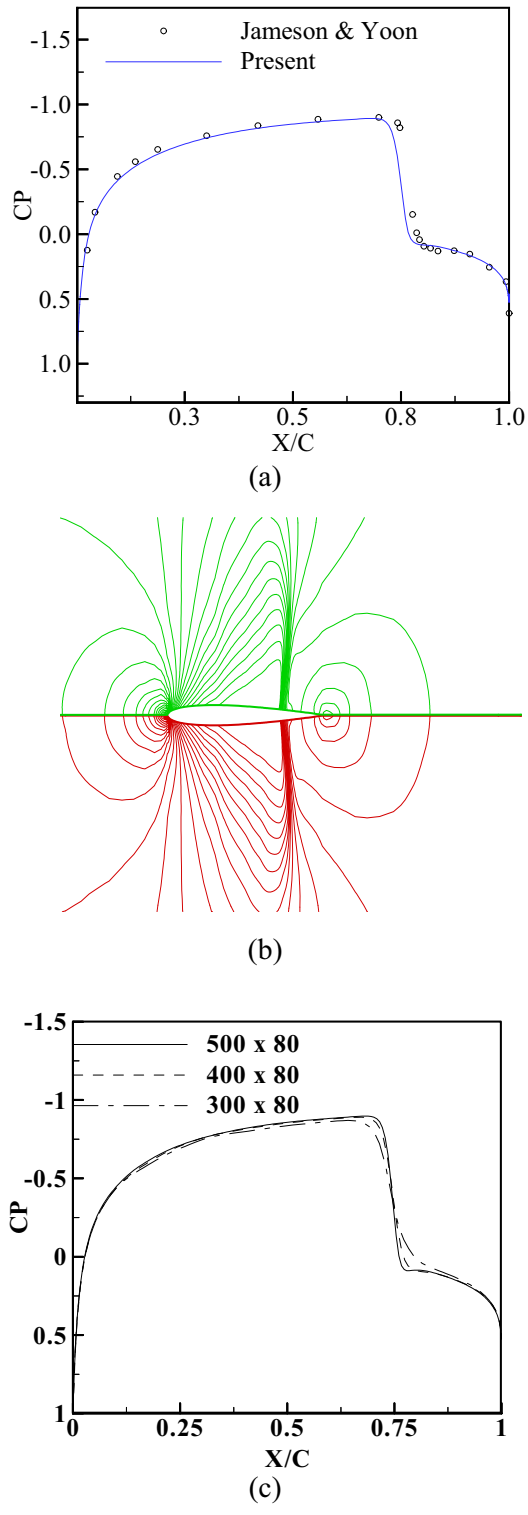

Figure 9 : (a) Surface pressure coefficient distribution (b) Pressure coefficient contours (c) Grid dependence test for α=0 and M_∞=0.85

wave. The Mach contour distributions and convergence histories for the three equations are shown in Figs. 5(e) and 5(f), respectively.

As anticipated, the proposed pressure based method has been also applied to many airfoil flow cases. Figs. 6(a) and 6(b) display the global view of the computational domain and enlargement of regions close to the surface of a NACA0012 airfoil, respectively. As it can be seen, a non-uniform grid in which the grid lines are closely packed near the airfoil surface is chosen. The value of K in SBIC method for all cases is 0.2, and the SBIC scheme for these cases is applied in prediction and correction steps.

Figs. 7 and 8 show computed results for free stream Mach number $M_{-\infty}$= 0.281 with $\alpha = 0$ and $\alpha = 4$ on a 255×83 grid, respectively. The pressure distribution coefficient on the upper and lower surface of the airfoil and the contours of the pressure coefficient for two attack angles are shown in Figs. 7(a), 7(b), 8(a) and 8(b).

The present results with pressure based algorithm and SBIC scheme are compared with experimental results [Neel (1997)]. These comparisons are considerable.

The third external case considered is transonic flow around the aforementioned NACA 0012 airfoil in a free stream with Mach number M=0.85, and angle of attack α=0 deg. The far-field boundary placed at 15 chord lengths away from the airfoil surface and a grid with 500×80 nodes are used. The distribution of pressure coefficients on the upper surface of the airfoil and the contours of pressure coefficient are shown in Figs. 9(a) and 9(b) respectively. The present results are compared with numerical data [Rizzi (1984)]. It can be seen that the computed results show good agreement.

A sharp discontinuity is achieved successfully for both shock strength and location. The grid dependence test is indicated in Fig. 9(c). As can seen, the results of these meshes do not change much, indicating that an acceptable solution can be obtained even on the coarse mesh. Also, aerodynamic coefficients for this case are presented in Tab. 1. Accuracy of these coefficients is good.

The fourth external case is transonic flow around the NACA0012 airfoil at M=0.85, α=1 deg. The number of nodes is the same as the previous case. For this case the distribution of pressure coefficient on the upper and lower surfaces of the airfoil and the contours of pressure coefficient are shown in Figs. 10(a) and 10(b), respectively. The results are compared with those of Zhou &

Table 1 : Aerodynamic coefficients NACA0012: M_∞= 0.85, α= 0

C_M	C_D	C_L	Method
0	0.0471	0	Rizzi(1984)
0	0.0559	0	Zhou & Davidson(1995)
0.001	0.047	-0.002	Present
0	0.049	0	Djavareshkian & Baheri (2004) (H grid)

Table 2 : Aerodynamic coefficients NACA0012: M_∞= 0.85, α=1

C_M	C_D	C_L	Method
-0.1282	0.0662	0.3890	Zhou & Davidson(1995)
-	0.0418	0.3520	Dervieux & Debiez (1996)
-	0.0582	0.3861	Jameson (1998)
-0.1166	0.0576	0.3700	Present
-0.119	0.0584	0.331	Djavareshkian & Baheri (2004)

Table 3 : Aerodynamic coefficients NACA0012 M_∞ = 0.8, α= 1.25

CM	CD	CL	Method
-0.0377	0.023	0.3513	Rizzi (1984)
-0.0375	0.022	0.3575	Zhou & Davidson (1995)
-	0.0232	0.3654	Jameson (1998)
-0.0320	0.0255	0.3281	Present
-0.041	0.025	0.334	Djavareshkian & Baheri (2004)

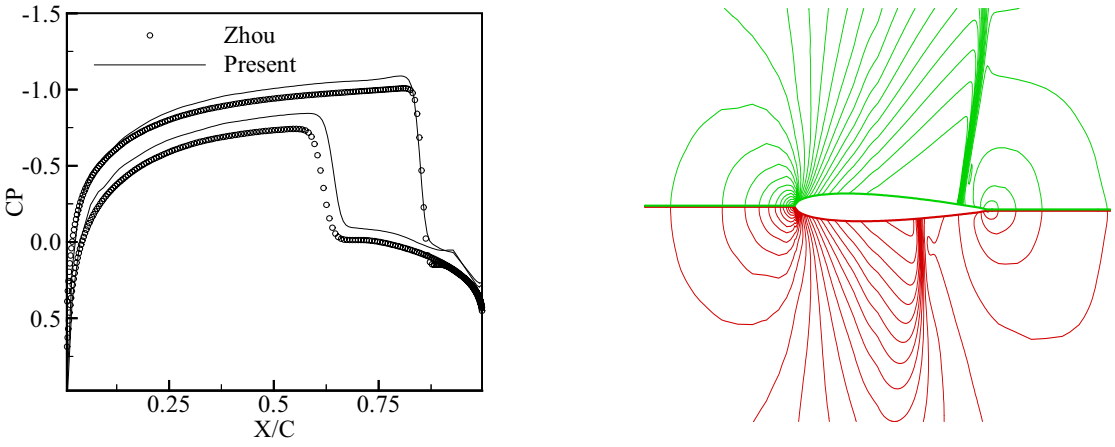

(a) (b)

Figure 10 : a) Surface pressure coefficient distribution b) Pressure coefficient contours for α=1 and M_∞=0.85.

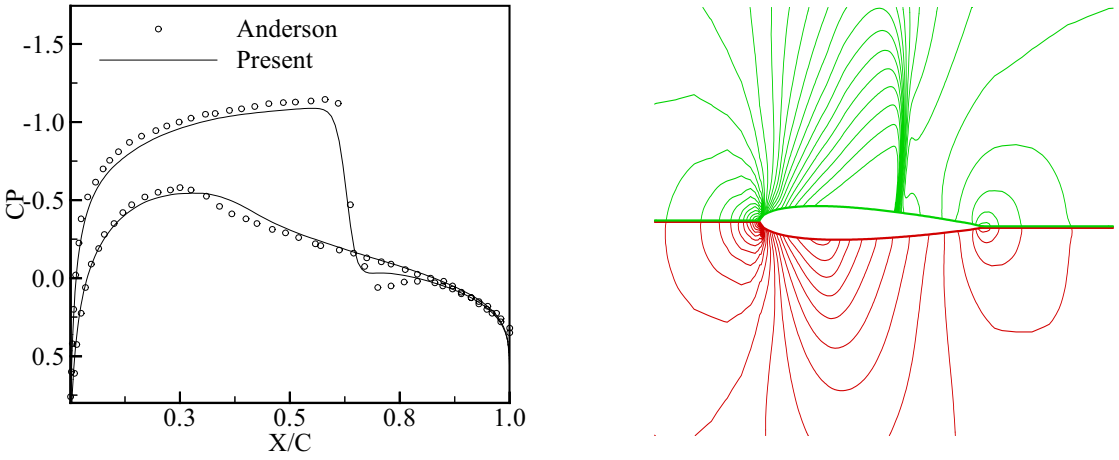

(a) (b)

Figure 11 : a) Surface pressure coefficient distribution b) Pressure coefficient contours for α=1.25 and M_∞=0.8.

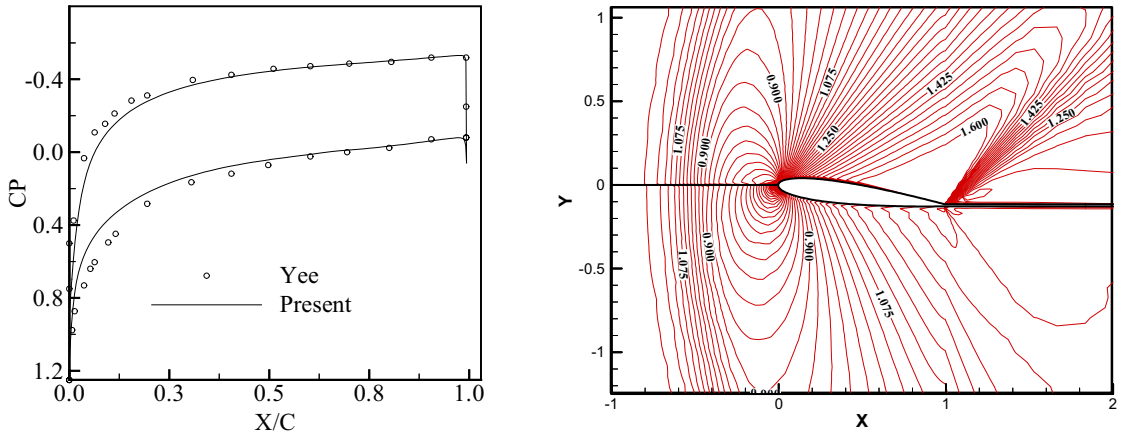

(a) (b)

Figure 12 : a) Pressure coefficient b) Mach contours for the NACA airfoil withM_∞=1.2, α=7

Davidson (1995). Also, aerodynamic coefficients for this case are presented in Tab. 2. These comparisons are considerable.

Fifth external case is for M=0.8, α=1.25 deg and with the same previous grid. The distribution of pressure coefficient on the upper and lower surface of the airfoil and the contours of pressure coefficient are shown in Figs. 11(a), 11(b). In this case results are compared with those of Anderson (1986). Also, aerodynamic coefficients for this case are presented in Tab. 3. This comparison shows the results (especially shock gradients) of the present scheme are considerable

Finally, Fig. 12 shows the results for the pressure coefficient distribution and the Mach contours for a supersonic external flow with $M_{-\infty}$=1.2, $\alpha = 7$. The present results with pressure based algorithm are compared with the results of Yee (1986) based on density based algorithm and TVD scheme. The comparison is considerable. Both bow shock as well as typical fishtail shock are shown in these figures. Note that the predicted bow shock is thicker than it should be. This is due to insufficient mesh resolution in this region. The sharp tail shocks are reasonably well captured.

6 Conclusions

In this paper, a high-resolution scheme has been developed in the context of an existing finite-volume procedure that uses a nonorthgonal mesh, and a pressure correction type of solution algorithm. A scheme based on normalized variable has been introduced to calculate the velocity component and energy; this scheme is also used to calculate interface density values in the correction step.

The method has been applied to internal and external flows and the results have been compared with predicted data by either other bounded schemes or experimental values. These comparisons show 1- when the present scheme is used in prediction and correction steps, the results of transonic and supersonic cases are better than those obtained by limiting the scheme to the prediction step. 2- the present bounded scheme predicts shock waves with high accuracy in internal and external flows 3- the proposed scheme can be used in compressible and incompressible flows. 4- the agreement between the results of the SBIC scheme in the pressure based algorithm and TVD schemes (in density-based methods) is excellent.

References

Anderson, W. K.; James, L. T. (1986): Comparison of Finite Volume Flux Vector Splittings for the Euler Equations. *AIAA Journal*, Vol. 24, No. 9: 1453 – 1460.

Batten, P.; Lien, F. S.; Leschziner M. A. (1996): A Positivity-Preserving Pressure-Correction Method", *Proceedings of 15th International Conf. On Numerical Methods in Fluid Dynamics*, Monterey, CA

Chakravarthy, S.R.; Osher S. (1983): High Resolution Application of the Osher Upwind Scheme for the Euler Equations, *AIAA Paper* 83-1943

Corol, S.; Jerome, H.; Katsuyoshi, N. (2004): Repair of Fatigued Steel Bridge girders with Carbon Fiber Strips, *University of Minnesota Report*, Department of Civil Engineering, 500 Pillsbury Drive S.E Minneapolis, MN 55455, Report No. MN/RC-2004-02

Darwish, M.S. (1993): A New High-Resolution Scheme based on the Normalize Variable Formulation, *Numerical Heat Transfer*, Part B, Vol.24, pp.353-371

Darwish, M.S.; Moukalled, F. H. (1994): Normalized Variable and Space Formulation Methodology for High-Resolution Schemes, *Numerical Heat Transfer*, Part B, 26: 79-96, 3-4: 169 - 188.

Deo, R.B.; Starnes, J.H.; Holzwarth, R.C (2001): Low-Cost Composite Materials and Structures for Aircraft Applications

Dervieux, A.; Debiez, C. (1996): Application of Mixed Element-Volume Muscl Method with 6th Order Viscosity Stabilization to Steady and Unsteady Flow Calculation. *Proceeding of Computational Fluid Dynamics*. John Wiley & Sons Ltd

Djavareshkian, M.H. (2001): A New NVD Scheme in Pressure-Based Finite-Volume Methods. 14th *Australasian Fluid Mechanics conference*, Adelaide University, Adelaide, Australia, pp. 339-342

Djavareshkian, M.H.; Baheri Islami, S. (2004): Transonic Turbulent Flow Simulation Using Pressure-Based Method And Normalized Variable Diagram, *International Journal of Engineering*, Transactions B, Vol. 17, No. 3, pp.

Gaskell, P.H.; Lau, A.K.C. (1988): Curvature-Compensated convective Transport: SMART, a New Boundedness-Preserving Transport Algorithm", *International Journal for Numerical Methods in Fluid*, Vol.8, pp.617-641

Issa, R. I. (1985): Solution of the Implicitly Discretized Fluid Flows Equations by Operator-Splitting, *Journal of Computational Physics*, Vol. 62, pp.40-62

Issa, R. I.; Lockwood, F.C. (1977): On the Prediction of Two–Dimensional Supersonic Viscous Interactions Near Walls, *AIAA Journal*, Vol. 15. No.2, pp. 182-188

Issa R.I.; Javareshkian M.H. (1998): Pressure-Based Compressible Calculation Method Utilizing Total Variation Diminishing Scheme, *AIAA Journal*, Vol. 36, No.9, pp.1652-1657

Jameson, A.; Martinelli, L. (1998): Mesh Refinement and Modeling Errors in Flow Simulation. *AIAA J.*, Vol.36, No.5.

Jasak, H.; Weller, H.G.; Gosman, A.D. (1999): High Resolution NVD Differencing Scheme for Arbitrarily Unstructured Meshes. *Int. J. Numer. Meth. Fluids* 31: 431-449

Karki, K.C.; Patankar, S.V. (1989): Pressure Based Calculation Procedure for Viscous Flows at All Speeds in Arbitrary Configurations, *AIAA Journal*, Vol. 27, No. 9, pp. 1167-1176

Kobyashi, M. H.; Pereira J. C. F. (1996): Characteristic-Based Pressure Correction at all Speed", AIAA Journal, Vol.34, No.2, pp.272-280

Leonard, B.P. (1983): Numerical Methods in Laminar and Turbulent Flows, *Pinerdge Press*, Swansee, U.K

Leonard B.P. (1988): Simple High-Accuracy Resolution Program for Convective Modeling of Discontinuities, *International Journal for Numerical Methods in Fluids*, Vol.8, pp.1291-1318

Lien, F. S.; leschziner, M. A. (1993): A Pressure-Velocity Solution Strategy for Compressible Flow and Its Application to Shock/Boundary-Layer interaction Using Second-Moment turbulence Closure, *Journal of Fluids Engineering*, Vol. 115. , pp. 717-725

McGuirk, J. J.; Page, G. L. (1990): Shock Capturing Using a Pressure-Correction Method, *AIAA Journal*, Vol. 28, No. 10, pp.1751-1757

Neel, R.E. (1997): Turbulent separated flows and transonic potential flows*, A dissertation submitted to the faculty of Virginia polytechnic institute and state university in partial fulfillment of the requirements for the degree of doctor of philosophy in aerospace engineering*.

Patankar, S. V.; Spalding, D. B. (1972): A Calculation Procedure for Heat Mass and Momentum Transfer I Three-Dimensional Parabolic Flows, *International Journal of heat and Mass Transfer*, Vol. 15, pp. 1782.

Rizzi, A. (1984): Spurious Entropy and Very Accurate Solutions to Euler Equations., *AIAA Paper*, 84 –1644.

Roe, P.L.; Enquist, E.; Osher, S.; Sommerville, R.J.C. (1985): Large Scale Computations in Fluid Mechanics, Part 2 (Lectures in Applied Mathematics, Vol. 22) *Springer Verlag,* pp. 163-193

Rubin, S.G.; Khosla, P.K. (1982): Polynomial Interpolation Method for Viscous Flow Calculations, *J. Comput. Phys*., Vol.27, pp.153-168

Sean, C.J.; Scott, A.C. (2003): Application of Fiber-Reinforced Polymer Overlays to Extend Steel Fatigue Life, *Journal of Composites for Construction* Vol.7, No. 4, pp.331-338

Shyy, W. (1988): A numerical Study of Two-Dimensional Compressible Navier-Stokes Flows, *Numerical Heat Transfer*, Vol. 14, pp.323-341

Shyy, W.; Thakur, S. (1994): Controlled Variation Scheme in a Sequential Solver for Recirculating Flow, *Heat Transfer*, Vol.25, No. 3, Pt. B, pp.273-286

Sujit, D. (2004): Automotive Lightweight Materials, *National Transportation Research Center*, 2360, Cherahala Boulevard Knoxville, FY 2004 Progress Report. T.N 37932-6472

Thukur, S.; Wright, J.; Shyy, W.; Liu, J.; Ouyang, H.; Vu, T. (1996): Development of Pressure-Based Composite Multigrid Methods for Complex Fluid Flows, *Progress in Aerospace Sciences*, Vol.32, No. 4, pp.313-375

Van Doormaal, J. P.; Raithby, G.D. (1984): Enhancement of the SIMPLE Method for Predicting Incompressible Fluid Flows, *Numerical Heat Transfer*, Vol.7, pp.147

Van Doormaal, J. P.; Raithby, G.D; McDonald, B.H. (1987): The Segregated Approach to Predicting Viscous Compressible Fluid Flows, *Journal of Turbomachinery*, Vol. 109, pp.268-277

Van Leer, B. (1974): Towards the Ultimate Conservative Difference Scheme, *J. Comput. Phys*., Vol. 14, pp.361-370

Van Leer, B. (1979): Towards the Ultimate Conservative Difference Scheme. V. A Second Order Sequel to Godunov's Method. *Journal of Computational Physics*, Vol.32, pp.101-36

Yee, H.C. (1986): Linearized form of Implicit TVD Schemes for the Multidimensional Euler and Navier-Stokes Equations, *Comp & Maths. With Appls*. Vol. 12A, Nos. 4/5, pp.413-432

Zhou, G. and Davidson, L., (1995): A Pressure Based Euler Scheme for Transonic Internal and External flow Simulation . *Int, J. Comp. Fluid Dynamics*, Vol. 5, No. 3-4: 169 - 188.

Zhu, J.; Rodi, W. (1991): A Low Dispersion and Bounded Convection Scheme, *Computer Methods in Applied Mechanics and Engineering,* Vol. 92, pp.87-96

Ziman, H. (1991): A Computer Prediction of Chemically Reacting Flows in Strirred Tanks, *PhD thesis*, University of London

Experimental Data Base for Computer Program Assessment, Tech.rep.,*AGARD Advisory* Rport No.138